Вычислительные технологии, 2021, том 26, № 5, с. 30–51. © ФИЦ ИВТ, 2021 ISSN 1560-7534
Computational Technologies, 2021, vol. 26, no. 5, pp. 30–51. © FRC ICT, 2021 eISSN 2313-691X

MATHEMATICAL MODELLING

DOI:10.25743/ICT.2021.26.5.004

# Generalized staircase model of electrochemical impedance of pores in supercapacitor electrodes

Pronkin Sergey N.[1], Shokina Nina Yu.[2]
[1]Institute of Chemistry and Processes for Energy, Environment, and Health, 67087, Strasbourg, France
[2]Medical Center — University of Freiburg, 79106, Freiburg, Germany
*Corresponding author: Pronkin Sergey N., e-mail: sergey.pronkin@unistra.fr
*Received September 13, 2021, accepted September 21, 2021.*

A new generalized staircase model of the electrochemical impedance is presented for porous electrode materials in energy storage devices. A brief overview on existing models of interfacial impedance and their limitations is given. The new model is based on the conventional staircase model of the impedance in cylindrical pores. However, the new model takes into account the complex porous structure of electrode materials. In particular, the impedance of hierarchical branching porous electrodes is described, i. e. the wide pores branching into the narrower pores. The new model allows to evaluate the impedance of the electrode/electrolyte interface in the presence of both non-faradaic and faradaic processes. The model is validated using the available exact solutions and experimental data for simple pore geometries. The influence of the parameters of structure of model porous electrodes on their performance in supercapacitors is studied. In particular, the influence of the diameter of the pores, width of pore openings, branching of pores is analyzed. The guideline for focused design of electrode materials of supercapacitors is outlined.

*Keywords*: staircase model, interfacial impedance, recursive equations, model systems.

*Citation*: Pronkin S.N., Shokina N.Yu. Generalized staircase model of electrochemical impedance of pores in supercapacitor electrodes. Computational Technologies. 2021; 26(5):30–51. DOI:10.25743/ICT.2021.26.5.004.

## Introduction

Transition toward the renewable energy sources is an important challenge of the present days. Renewable solar and wind energy sources are intermittent by character, therefore their utilization requires reversible and efficient energy storage devices [1]. Electrochemical energy storage devices (EESD), such as batteries and supercapacitors, are among the most efficient and environmentally friendly existing energy storage technologies. In particular, supercapacitors have significantly higher power output and longer cycle life, but lower energy density, comparing to modern batteries [2].

The performance of supercapacitors depends on the properties of their electrode materials, in particular, on the charge capacitance, mass specific and volume specific capacitances,

and material response rate to voltage modulation [3]. Understanding the dependence of these parameters on the structural characteristics of electrode materials, such as porosity and specific surface area (SSA) is important for the focused design of new materials with improved electrochemical performance.

The electrochemical performance of supercapacitor electrode materials is determined by the characteristics of physicochemical processes on electrode/electrolyte interface. Therefore, studying these characteristics is vitally important for designing electrode materials with strong electrochemical performance.

The electrochemical impedance spectroscopy is a powerful tool for studying the processes on electrode/electrolyte interface [4]. Measuring the impedance spectra, i. e. the interfacial impedance dependency on the frequency of potential modulation, allows to probe the parameters of various interfacial processes occurring at different rates. The extraction of the characteristics of interfacial processes from experimental impedance spectra requires proper mathematical models.

For a flat electrode, there exist simple mathematical models with analytical solutions. However, for the electrode materials with complex geometries, such as porous electrodes of supercapacitors, there was no mathematical model, which could take into account the complex porous structure of the material.

The current work presents the generalized staircase model, which is a new multi-parametric mathematical model of an interfacial impedance of porous electrode materials. The model takes into account the parameters of complex pore structure, such as diameter and length of the pores, their geometry and branching. The model can be adapted to describe various interfacial processes, such as adsorption/desorption and electrochemical reactions.

The model is validated using the available exact solutions and experimental data for simple pore geometries. This allows applying the model to complex structures with several pore types and multiple pore branching. The influence of various structural parameters on the impedance is studied and the guideline for focused design of electrode materials of supercapacitors is outlined.

The paper is organized as follows. The first section reviews the mathematical models of interfacial impedance for various interfacial processes, such as adsorption, charge transfer and diffusion. The limitations of existing models are discussed. In the second section the generalized staircase model of interfacial impedance for electrodes with complex porous structures in the presence of various interfacial processes is presented. The third section presents the model validation and its application to complex porous structures. The influence of various parameters of porous structure on electrochemical performance of materials in supercapacitors is evaluated.

## 1. Models of interfacial impedance

Electrochemical impedance measurement is a powerful tool to study the properties of electrode/electrolyte interface, in particular, the interfacial capacitance. The electrochemical impedance $\mathbf{Z}$ is measured as a function relating the electrochemical potential $\mathbf{E}$ and the electrical current $\mathbf{I}$ passing through the interface:

$$\mathbf{E}(\omega) = \mathbf{Z}(\omega) \times \mathbf{I}(\omega). \tag{1}$$

Generally, a small periodic modulation of electrode potential $\mathbf{E} = E_0 \cdot \sin(\omega t)$ is applied and the current through electrode/electrolyte interface $\mathbf{I} = I_0 \cdot \sin(\omega t + \phi)$ is measured. Here

$\omega = 2\pi f$ is the angular frequency, $f$ is the modulation frequency and $\phi$ is the phase shift angle between $\mathbf{E}$ and $\mathbf{I}$.

In order to obtain the characteristics of interfacial processes with various rates, the impedance $\mathbf{Z}$ is measured at various modulation frequencies $f$. Typically, the impedance diagrams are presented in the form of Nyquist plots ($-\mathrm{Im}(\mathbf{Z})$ vs $\mathrm{Re}(\mathbf{Z})$) or Bode plots ($\log|\mathbf{Z}|$ vs $\log f$). The analysis of impedance spectra allows to identify the processes taking place on the interface and to evaluate their characteristics by applying a corresponding mathematical model of impedance.

### 1.1. The impedance of the processes on a flat electrode/electrolyte interface

First, the impedance of a flat electrode/electrolyte interface will be presented below, which allows to neglect the influence of the geometry of the interface. This influence will be discussed later in the next subsections.

A modulation of electrode potential can result in a number of interfacial processes. In supercapacitor electrodes, two types of interfacial processes occur: ions adsorption/desorption and interfacial charge transfer. The interfacial processes are also classified as non-faradaic and faradaic. In non-faradaic process, neither electrolyte species, nor electrode components change their oxidation states, i. e. no electrochemical reduction-oxidadion (redox) faradaic process takes place.

Below the impedance models of the interfacial processes typical for supercapacitor electrodes are presented.

#### 1.1.1. Non-faradaic adsorption/desorption of electrolyte species on electrode surface

Adsorption of ions on electrode surface results in the formation of electrical double layer (EDL) [5] and a charge accumulation on the interface, similar to a capacitor. Thus, the interfacial impedance of this process is given by:

$$\mathbf{Z}_C = \frac{1}{i\omega C_{dl}}. \tag{2}$$

Here $C_{dl}$ is the so-called double layer capacitance [5]. For a flat electrode/electrolyte interface, $C_{dl}$ can be calculated by the equation for the capacitance of a 2-plate capacitor:

$$C_{dl} = \frac{\varepsilon\varepsilon_0 A}{d} = C_s A. \tag{3}$$

Here $\varepsilon$ is the apparent dielectric constant of the interface, $d$ is the thickness of the EDL, $A$ is the surface area of the interface. $C_s$ is the surface specific interfacial capacitance, which depends on the nature of the interface. Generally, $C_s$ is found in the range of 5–30 $\mu\mathrm{F/cm}^2$.

The equation (2) shows that for $\mathbf{Z}_C$ phase angle $\phi = 90°$ (the curve *1* in Fig. 1). $C_{dl}$ value can be calculated by fitting the experimental data $\mathbf{Z}$ using (2).

#### 1.1.2. Interfacial charge transfer: Faradaic interfacial reaction

If at least one component of electrolyte or electrode changes its oxidation state due to the potential modulation, the redox faradaic process takes place at the electrode/electrolyte interface:

$$\mathrm{Ox} + \mathrm{ne}^- \underset{\longleftarrow}{\overset{k_0}{\rightleftharpoons}} \mathrm{Red}. \tag{4}$$

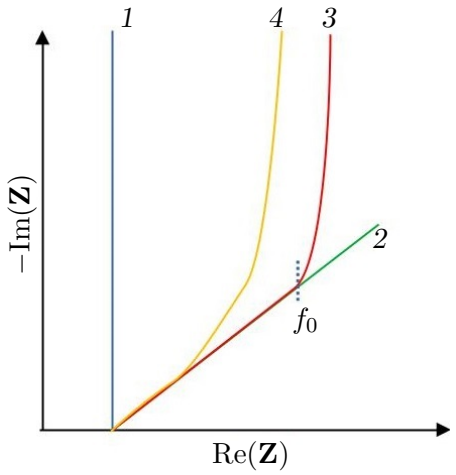


Fig. 1. The schematic representation of the Nyquist diagram for the non-faradaic impedance $\mathbf{Z}_C$ of: *1* — the flat electrode (2); *2* — the semi-infinite cylindrical pore; *3* — the finite cylindrical pore; *4* — the electrode with pores of different diameters

If the electrode potential is close to the equilibrium potential $E^0_{\mathrm{Ox/Red}}$, then for a small potential modulation, $\mathbf{I}$ changes linearly with $\mathbf{E}$ similar to Ohm's law. Thus, the impedance of interfacial charge transfer can be approximated by the charge transfer resistance $R_{ct}$ with $\phi = 0$:

$$R_{ct} = \frac{RT}{nFi_0}. \tag{5}$$

Here $i_0$ is the exchange current rate, which is related to the kinetic parameters of the reaction (4):

$$i_0 = FAk_0 C_{\mathrm{Ox}}^{1-\alpha} C_{\mathrm{Red}}^{\alpha}, \tag{6}$$

where $C_{\mathrm{Ox}}$ and $C_{\mathrm{Red}}$ are the concentrations of Ox and Red in the electrolyte, $\alpha$ is the symmetry factor for the reaction (4), $0 < \alpha < 1$, $k_0$ is the heterogeneous rate constant of the reaction (4).

According to (5), (6), the value of $R_{ct}$ depends on the concentration of Ox and Red. If the reaction (4) is fast, then the interfacial concentrations of reagents are not the same as in the electrolyte. The rate of the fast reaction (4) is influenced by the diffusion rate of reagents to/from the interface. This influence is reflected in the appearance of an additional component of impedance in the serial combination with $R_{ct}$, namely, the Warburg impedance $\mathbf{Z}_W$:

$$\mathbf{Z}_f = R_{ct} + \mathbf{Z}_w, \tag{7}$$

$$\mathbf{Z}_w = \frac{\sigma}{\sqrt{\omega}} + \frac{\sigma}{i\sqrt{\omega}}. \tag{8}$$

The parameter $\sigma$ is called the Warburg constant and related to the parameters of ion diffusion in the electrolyte:

$$\sigma = \frac{RT}{n^2F^2A\sqrt{2}} \left( \frac{1}{C_{\mathrm{Ox}}\sqrt{D_{\mathrm{Ox}}}} + \frac{1}{C_{\mathrm{Red}}\sqrt{D_{\mathrm{Red}}}} \right). \tag{9}$$

Here $D_{\mathrm{Ox}}$ and $D_{\mathrm{Red}}$ are diffusion coefficients of Ox and Red in the electrolyte.

From (8) it can be seen that the Warburg impedance $\mathbf{Z}_w$ has the phase angle $\phi = 45°$, because $\mathrm{Re}(\mathbf{Z}_w) = \mathrm{Im}(\mathbf{Z}_w)$.

### 1.1.3. Impedance of the interfacial charge storage

The interfacial impedance depends on the processes taking place on the interface, both faradaic and non-faradaic. The formation of the EDL is one of main mechanisms of charge storage in the supercapacitors. In particular, supercapacitors relying on non-faradaic mechanisms of charge storage (namely, ions adsorption) are called electrochemical double-layer capacitors (EDLC). A typical electrode material in EDLC is the porous carbon with very high specific surface area, in general above 2000 $m^2/g$. These materials demonstrate high conductivity and electrochemical stability, resulting in high power output, short charging times and long cycling life. However, their specific energy density is limited due to a low surface specific capacitance of the carbon surface $C_s \approx 5\ \mu F/cm^2$. Thus, the specific capacitance of carbon electrode materials seldom exceeds 200 F/g.

In order to overcome the limitations related to the low surface specific capacitance $C_s$, the materials with faradaic mechanism of charge storage are utilized. In particular, nanoparticles of transition metal oxides (TMO) can be deposited on carbon surface. In general, TMO have a much higher surface specific capacitance due to the phenomena of electrolyte ion intercalation into the bulk of oxide particles. This mechanism of charge storage in the oxide materials is known as pseudocapacitance. The pseudocapacitance results in charge accumulation in electrode materials due to ion intercalation, retarded by slow kinetics of interfacial ion charge/discharge. The devices utilizing these types of materials are called pseudocapacitors.

If no faradaic reaction occurs on a flat electrode/electrolyte interface, then its impedance can be modelled as a serial combination of $R_1$ and $C_{dl}$, where $R_1$ depends on the conductivity of an electrolyte and geometry of the electrochemical system. $R_1$ contains no information on interfacial processes. $R_1$ can be easily measured as a limit of $\mathbf{Z}(\omega)$ at high $f$ and subsequently excluded from the further analysis.

If a redox process occurs on the interface, then the interfacial impedance includes a faradaic impedance component $\mathbf{Z}_f$. At a small potential modulation, $C_{dl}$ and $\mathbf{Z}_f$ can be considered as independent components. Therefore, the interfacial impedance can be modelled as their parallel combination (Fig. 2, *a*).

The simplest case of a faradaic process is the reversible electrochemical reaction. This reaction is controlled by its kinetics and the diffusion of electrolyte components. Therefore,

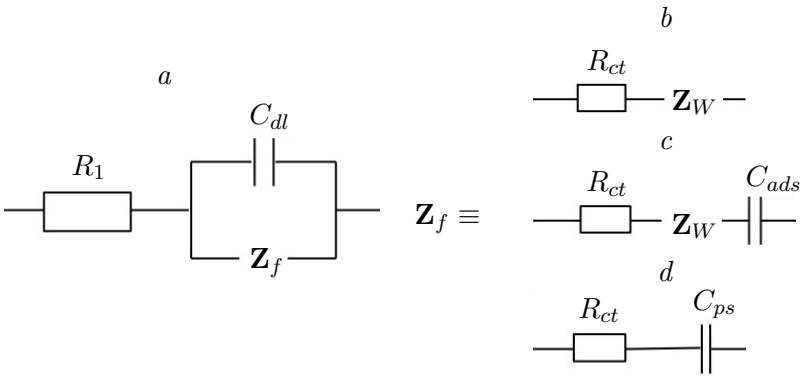


Fig. 2. *a* — The model equivalent circuit of the impedance of the flat electrode/electrolyte interface in the presence of a faradaic process. The models of the faradaic impedance $\mathbf{Z}_f$: *b* — the Randles model; *c* — the Melik – Gaykazyan model; *d* — pseudocapacitance model

$\mathbf{Z}_f$ is modelled by the Randles circuit (Fig. 2, *b*). The circuit consists of a serial combination of 2 components: $R_{ct}$ and $\mathbf{Z}_W$.

The Randles model predicts that $\lim\limits_{\omega\to\infty}(\mathbf{Z}) = R_1$ and $\lim\limits_{\omega\to 0}(\mathbf{Z}) = R_1 + R_{ct} + Z_w$. This behavior was observed, for example, for the reversible redox transformation of the $Fe^{II}/Fe^{III}$-cyanide complex on the Au polycrystalline electrode [13]. Fitting the experimental impedance spectra by the Randles model allows to determine $k_0$, $D_{\mathrm{Ox}}$ and $D_{\mathrm{Red}}$ for a reversible faradaic process on the flat electrode.

For more complex reactions, the advanced models of faradaic impedance have to be used. For example, if the reaction involves the formation of adsorbed intermediate, then the reaction results in accumulation of charge on the interface and adds a capacitive component to $\mathbf{Z}_f$. The impedance of this process is described by the Melik – Gaykazyan model impedance [6] (Fig. 2, *c*).

The interfacial faradaic impedance related to the pseudocapacitance can be modelled as a serial combination of $R_{ct}$, related to the slow kinetics of interfacial reaction (5), and $C_{ps}$, related to the capacitance of ions intercalation (Fig. 2, *d*).

### 1.2. Models of impedance of porous electrodes

The models from Subsection 1.1.3 describe the impedance of a flat uniform electrode/electrolyte interface, for which the current lines are parallel, evenly distributed, and perpendicular to the interface. However, the materials with rough surfaces and the porous materials are commonly used in the EESD in order to increase surface and volume specific energy densities.

In order to model the impedance of supercapacitor electrodes, the influence of porous structure has to be taken into account for any mechanism of the interfacial charge storage. The impedance of the interface inside a pore is often modelled by the staircase-type equivalent circuit (Fig. 3).

According to the DeLevi theory [4], for the infinitely long cylindrical pore, the interfacial impedance is described by the following equation:

$$\mathbf{Z}_p = \sqrt{R|\mathbf{Z}|}e^{i\phi/2}. \tag{10}$$

Here $R$ is the electrolyte resistance per unit length within the pore, $\mathbf{Z}$ is the impedance of the pore wall/electrolyte interface, $\phi$ is the phase angle of $\mathbf{Z}$. (10) predicts that the interfacial

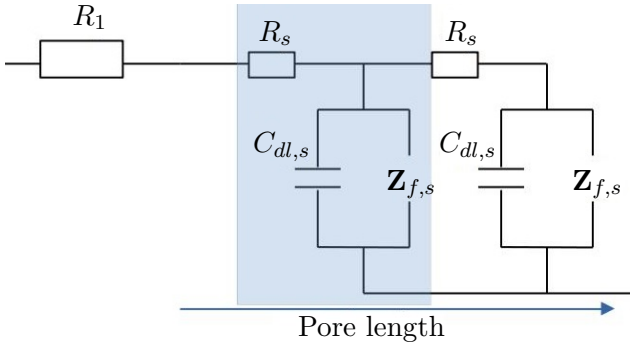


Fig. 3. The staircase equivalent circuit of the impedance model for a single pore. The highlighted elements form the repeating pattern along the pore

impedance inside the pore has the phase angle equal to the half of the impedance of a flat electrode. For example, for the non-faradaic impedance $\mathbf{Z}_{nf}$ the DeLevi model (10) predicts a constant phase angle $\phi = 45°$.

When applying the staircase model to the analysis of a pore with a finite length $l_p$, it is convenient to define a length $\lambda$ of the penetration of the potential modulation into the pore [8]:

$$\lambda = \frac{1}{2}\sqrt{\frac{\sigma d_p}{2\omega C_s}}. \tag{11}$$

Here $\sigma$ is the conductivity of the electrolyte (in $\mathrm{Ohm}^{-1}\cdot\mathrm{m}^{-1}$), $d_p$ is the pore diameter, and $C_s$ is the surface specific interfacial capacitance.

From (11) it follows that $\lambda$ increases with a decrease in the modulation frequency $f = \omega/2\pi$. Thus, $\lambda > l_p$ for the frequencies below a certain threshold $f_0$. If $\lambda > l_p$, then the potential modulation is uniform along the whole length of the pore, and the pore impedance is the same as the impedance of a flat electrode with the same surface area. In this case, one observes a change from the shift angle $\phi = 45°$ at $f > f_0$ to $\phi = 90°$ for $f < f_0$ in the Nyquist diagram (Fig. 1, *3*). This transition is often observed for the porous carbon electrodes (for example, in [15]). In general, the transition is much less sharp and occurs over a certain range of frequencies (see Fig. 1, *4*) due to the presence of the pores with various diameters and shapes [8, 9].

The staircase model (10) allows to correctly fit the experimental impedance spectra of the porous electrodes in the absence of faradaic processes and determine the capacitance $C_{dl}$. Moreover, the average pore length $l_p$ can be estimated from the $f_0$ value, providing that the average diameter $d_p$ of the pores is known from the other methods.

In the model (10) it is assumed that individual pores are not interconnected. Therefore, the staircase circuit is applied independently to each pore. The supercapacitors electrode materials, for example, the activated carbon, often have hierarchical pores: the larger pores branch into several smaller pores of next generation, which can branch further. The hierarchical porous structure makes the application of the staircase model more complicated, because the staircase circuits of pores from different generations are no longer independent.

The model of branching pores was proposed in [10] by introducing 2 generations of pores: the large ($\mu$m size) voids between carbon particles and the narrower (sub-$\mu$m size) internal pores. The larger pores were branching into $n$ smaller pores, and the length and diameter of smaller pores were scaled by $a_l$ and $a_d$ factors in comparison to the parent pores. Fitting the experimental spectra allowed to estimate the branching factor $n$ and scaling factors $a_l$, $a_d$. However, these values have to be considered as estimates only, because the porous structure is more complex.

The model [10] also demonstrates that the pores branching is counter-productive for efficient utilization of the capacitance of porous electrodes. Indeed, the capacitance of the interface of the porous electrode decreased in comparison to the capacitance of a flat electrode $C_{dl}$ with the increase of the branching factor $n$. This conclusion is an important guiding rule for material science in the optimization of the structure of electrode materials. However, the unambiguous analysis of the influence of various structural parameters is difficult because of their interdependence. In particular, in [10] the porosity of electrode material and the length scaling factor $a_l$ were fixed. The increase of the branching factor led to narrowing of the pores of the next generation. This narrowing led to the decrease of the modulation penetration depth (11), and, thus, to the decrease of the efficiency of pore surface utilization.

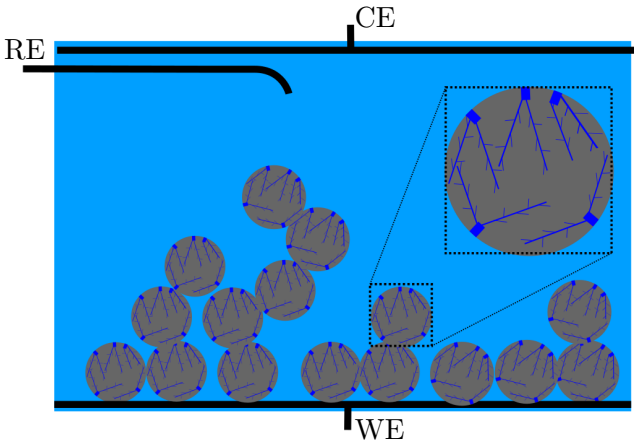


Fig. 4. The sketch of an electrode with the hierarchical porous structure with 3 generations of pores

It has to be mentioned that the model [10] assumed the serial connection of a parent pore and its branches: such as if the pores were branching only at their bottoms. This allowed to utilize the same polarization conditions for all pores of the same generation, thus, simplifying the model. In reality, however, the branches can appear over the whole length of a pore (Fig. 4).

In the following subsection the improved model of the impedance of a porous electrode is presented. This model utilizes a staircase circuit and takes into account the presence of 3 generations of branching pores. The model with 3 generations of pores describes well the structure of porous carbon electrode materials. However, it is important to note the model can be extended to include any number of pores generations. The pores of $2^{\text{nd}}$ and $3^{\text{rd}}$ generations are formed by branching a parent pore. The branches are uniformly distributed over the length of the parent pore. The faradaic impedance of pseudocapacitance is also included into the staircase model, allowing to describe the porous electrodes of pseudocapacitors. Thus, this new model is named as "generalized staircase model". The model is designed to predict the influence of the structural parameters of electrode materials on their performance in supercapacitors. Namely, the influence of the pores lengths and diameters, the porosity of the material, and the branching factors is evaluated.

## 2. Generalized staircase model

The sketch of the electrode material is depicted in Fig. 4. The material is assumed to have 3 hierarchical generations of pores. The pores of the $2^{\text{nd}}$ and $3^{\text{rd}}$ generations are the branches of the parent pores and evenly distributed over the length of a parent pore. The pores of $3^{\text{rd}}$ generation are terminal: they have no branches.

Each generation of the pores has 2 characteristic parameters: a pore length $l_{p,i}$ and a pore diameter $d_{p,i}$, where $i$ is a generation index. The surface area of the individual pore of the $i^{\text{th}}$ generation is given as

$$A_i = \pi d_{p,i} l_{p,i} + \frac{\pi d_{p,i}^2}{4}. \tag{12}$$

Neglecting the surface of the material outside the pores, the total surface area of the material is calculated as the surface area $A_p$ of all pores:

$$A_p = N_1(A_1 + \beta_{12}A_2 + \beta_{12}\beta_{23}A_3). \tag{13}$$

Here, $\beta_{12}$ and $\beta_{23}$ are the branching factors: $\beta_{12} = N_2/N_1$, $\beta_{23} = N_3/N_2$, where $N_1$, $N_2$, $N_3$ are the numbers of pores of the 1st, 2nd, and 3rd generations correspondingly. The factors $\beta_{12}$ and $\beta_{23}$ are the model parameters, whereas $N_1$ is calculated as

$$N_1 = \frac{m \cdot SSA}{A_1 + \beta_{12}A_2 + \beta_{12}\beta_{23}A_3}, \tag{14}$$

where $m$ is the mass of the deposit (in g), $SSA$ is the specific surface area of the electrode material (in $m^2/g$).

The impedance of the pores of each generation is modelled by the staircase circuit as described below.

### 2.1. Model of an individual pore of the 3rd (terminal) generation

The Fig. 5 shows the equivalent circuit utilized in the generalized staircase model for the impedance $\mathbf{Z}_{3g}$ of an individual pore of the 3rd generation (a pore with the smallest diameter and no branches). The pore is divided into $K = 2^n$ identical segments. The value $n = 10$ is used for all calculations, as it was found that further increase in $n$ does not change the results of modelling.

For the pore with the diameter $d_p$ and the length $l_p$, the length of a segment is $\delta_l = l_p/K$, the surface area of the walls of a segment is $A_s = \pi d_p \delta_l = \pi d_p l_p/K$, and the surface of the bottom of the pore is $A_b = \pi d_p^2/4$.

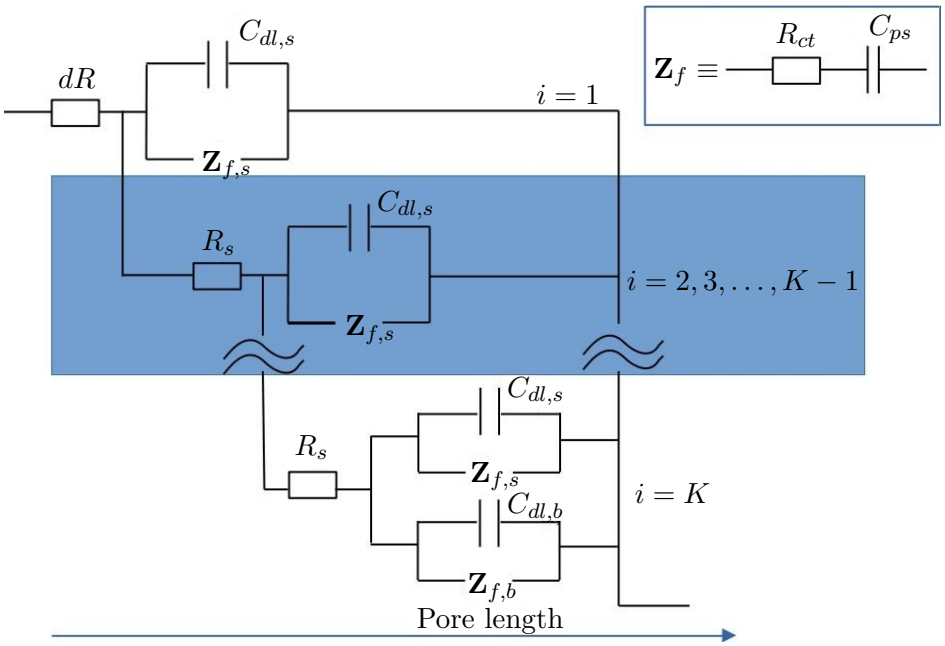


Fig. 5. The equivalent circuit applied in the generalized staircase model. The highlighted area corresponds to the repetitive pattern of the circuit. The inset depicts the model of the faradaic impedance related to the pseudocapacitance

A single segment has the interfacial impedance $\mathbf{Z}_s$. It is computed using the EDL capacitance $C_{dl,s}$ of the walls of the segment. If the model includes also a faradaic impedance, then the faradaic impedance $\mathbf{Z}_{f,s}$ of the segment walls is added in parallel to $C_{dl,s}$. Therefore, in the presence of pseudocapacitance the total impedance of the segment walls is given by the following equations:

$$\frac{1}{\mathbf{Z}_s} = \frac{1}{i\omega C_{dl,s}} + \frac{1}{\mathbf{Z}_{f,s}}, \tag{15}$$

$$C_{dl,s} = C_s A_s = C_s \pi d_p \frac{l_p}{K}. \tag{16}$$

The faradaic impedance $\mathbf{Z}_{f,s}$ is related to the pseudocapacitance and modelled as a serial combination of the charge transfer resistance $R_{ct,s}$ and the capacitance $C_{ps,s}$ (see the inset of Fig. 5):

$$\mathbf{Z}_{f,s} = R_{ct,s} + \frac{1}{i\omega C_{ps,s}}. \tag{17}$$

Both $R_{ct,s}$ and $C_{ps,s}$ are calculated for the whole surface area $A_s$ of the segment walls:

$$R_{ct,s} = \frac{RT}{nFi_0 A_s} = \frac{RTK}{\pi nFi_0 d_p l_p}, \tag{18}$$

$$C_{ps,s} = C_{ps} A_s = \pi C_{ps} \frac{d_p l_p}{K}. \tag{19}$$

The final segment of the pore contains the contribution from its walls ($\mathbf{Z}_s$) as well as the contribution from the pore bottom ($\mathbf{Z}_{s,b}$). The parameters of the impedance $\mathbf{Z}_{s,b}$ of the bottom, namely, $C_{dl,b}$ and $\mathbf{Z}_{f,b}$, are calculated using the equations same as (16)–(19), but with the bottom surface area $A_b$ instead of the wall surface area $A_s$.

Thus, the impedance $\mathbf{Z}_K$ of the last segment of the pore is calculated according to the circuit in Fig. 5 as follows:

$$\mathbf{Z}_K = R_s + \frac{1}{\dfrac{1}{\mathbf{Z}_s} + \dfrac{1}{\mathbf{Z}_{s,b}}}. \tag{20}$$

Here $R_s$ is the resistance of the electrolyte inside a segment of the pore:

$$R_s = \frac{1}{\sigma} \frac{\delta_l}{\pi d_p^2} = \frac{l_p}{\pi \sigma d_p^2 K}, \tag{21}$$

where $\sigma$ is the conductivity of the electrolyte.

The part of the pore containing last two segments ($K$ and $K-1$) has the impedance $\mathbf{Z}_{K-1}$:

$$\mathbf{Z}_{K-1} = R_s + \frac{1}{\dfrac{1}{\mathbf{Z}_s} + \dfrac{1}{\mathbf{Z}_K}}. \tag{22}$$

In general, the impedance of the part of the pore containing $i$ segments (counting from the bottom of the pore, i. e. segments from $i$ to $K$) is calculated by the recursive equation similar to (22):

$$\mathbf{Z}_i = R_s + \frac{1}{\dfrac{1}{\mathbf{Z}_s} + \dfrac{1}{\mathbf{Z}_{i+1}}}. \tag{23}$$

Thus the total impedance of a pore of the 3$^{\text{rd}}$ generation with $K$ segments is equal to the impedance of the pore with all segments from 1 to $K$: $\mathbf{Z}_{3g} = \mathbf{Z}_1$.

### 2.2. Impedance of pores of the 1st and 2nd generations

The impedance of the pores of the 1st and 2nd generations is calculated by the same generalized staircase model as for the pores of 3rd generation, except that the contribution of the impedance of the next generations is taken into account.

The interfacial impedance of each segment of the pores of the 1st and 2nd generations is modelled by the circuit depicted in Fig. 6.

For example, an individual pore of the 2nd generation is branched into $\beta_{23}$ pores of the 3rd generation. The total impedance of $\beta_{23}$ parallel pores with impedance $\mathbf{Z}_{3g}$ is equal to $\mathbf{Z}_{3g}/\beta_{23}$. It is assumed that the branch pores are uniformly distributed over the whole length of the parent pore. Thus, each segment of the parent pore contains an average additional impedance element $\mathbf{Z}^*$ due to the impedance of the next generation pores. For the pores of the 2nd and the 1st generations this additional element is given by the following corresponding equations:

$$\mathbf{Z}^*_{2g} = \frac{\mathbf{Z}_{3g}K}{\beta_{23}}, \tag{24}$$

$$\mathbf{Z}^*_{1g} = \frac{\mathbf{Z}_{2g}K}{\beta_{12}}, \tag{25}$$

where $\mathbf{Z}_{3g}$ and $\mathbf{Z}_{2g}$ are the total impedances of the individual pore of the 3rd or 2nd generation correspondingly.

Thus, according to the circuit in Fig. 6, the interfacial impedance $\mathbf{Z}_s$ of a segment of a pore of the 1st or 2nd generation is calculated as

$$\frac{1}{\mathbf{Z}_s} = \frac{1}{i\omega C_{dl,s}} + \frac{1}{\mathbf{Z}_{f,s}} + \frac{1}{\mathbf{Z}^*}, \tag{26}$$

where $\mathbf{Z}^*$ denotes $\mathbf{Z}^*_{1g}$ or $\mathbf{Z}^*_{2g}$ for the pores of 1st or 2nd generations correspondingly.

Physically, this approach to account for a contribution of the impedance of branch pores is equivalent to adding a branch pore with impedance equal to $\mathbf{Z}^*_{2g}$ or $\mathbf{Z}^*_{1g}$ to each of $K$ segments.

(26) differs from (15) for $\mathbf{Z}_s$ for the pores of 3rd terminal generation by the $1/\mathbf{Z^*}$ term. Besides this difference, the rest of the calculation of the impedance of an individual pore is the same for all generations.

Finally, the total impedance of all pores of the material is calculated as the total impedance of all $N_1$ pores of the 1st generation:

$$\mathbf{Z}_p = \frac{\mathbf{Z}_{1g}}{N_1}. \tag{27}$$

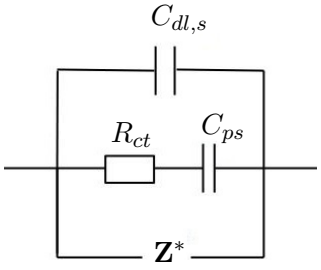


Fig. 6. The equivalent circuit modelling the interfacial impedance of a segment of an individual pore of the 1st and 2nd generations

A new generalized staircase model of the electrochemical impedance was implemented in the original software package "IMPerial", developed by the authors. "IMPerial" is a modular software for multiparametric modelling of interfacial impedance in the presence of various electrochemical phenomena.

## 3. Results and discussion

The parameters of the materials of the electrode and electrolyte utilized in the calculations are listed in Table.

$SSA$ = 230 $m^2/g$ is close to the value for the carbon Vulcan XC-72, often utilized as electrode material. This carbon black material consists of the small primary carbon particles (ca. 30 nm) filled by the micropores with an average diameter $d < 2$ nm [11]. The primary particles form the agglomerates with the size equal to 100–300 nm, which include the pores with the diameters equal to 2–20 nm. The agglomerates form the large ($\mu$m size) chain-like structures containing the macropores with the diameter $d > 50$ nm. Following this description, 3 types of pores of the model carbon material (see Fig. 4) can be considered as 3 generations in the generalized staircase model:

- micropores ($d_{p,3} = 0.7$ nm), representing the apex and terminal branches of the inner pores inside the primary particles;
- small mesopores ($d_{p,2} = 3$ nm), representing the major population of pores inside the primary particles;
- large mesopores ($d_{p,1} = 30$ nm), representing the opening mouth of the smaller mesopores and the zones of contacts between primary particles.

According to the classification of Eikerling [14], the diameters of the pores of the 1st and 2nd generations correspond to the secondary and primary pores of the carbon electrode materials in fuel cells. These pores are important for efficient accessibility of the electrode/electrolyte interface. In the generalized staircase model, the micropores (3rd generation) are also added, because their presence is known to be beneficial for the performance of the supercapacitors [12]. On the other hand, the presence of a large population of macropores ($d \approx 150$ nm) in Vulcan XC-72 is neglected. These macropores make a relatively small contribution to the overall SSA of the carbon material and behave as a flat electrode under the conditions of the potential modulation utilized in the EIS measurements.

The lengths of the pores of the 2nd and 3rd generations are the variables of the model. The length of large mesopores (1st generation) is fixed to 0.1 $\mu$m, i. e. these pores are relatively short and represent the openings of pores within the agglomerates. The macropores branch into narrower and longer (3 $\mu$m) mesopores of the 2nd generation.

The parameters of materials used in calculations

| Parameter | Value |
|---|---|
| $SSA$ | 230 $m^2/g$ |
| $\sigma$ | 2 $S \cdot m^{-1}$ |
| $C_s$ | 5 $\mu F/cm^2$ |
| $C_{ps}$ | 300 $\mu F/cm^2$ |
| $\rho_c$ | 2 $g/cm^3$ |
| $m$ | 1 g |

In order to evaluate the performance of a porous material as supercapacitor electrodes, the measurable capacitance of the material is calculated as $-1/\omega \cdot \mathrm{Im}(\mathbf{Z_p})$ and the surface specific calculated capacitance $C_{s,c}$ as

$$C_{s,c} = -\frac{1}{A_s}\frac{1}{\omega \cdot \mathrm{Im}(\mathbf{Z_p})}. \tag{28}$$

One of the main characteristics of the supercapacitor electrode material is the volume specific capacitance $C_V$ [2], because it depends on both surface specific capacitance $C_s$ and porosity of the material. Thus, $C_V$ is the outcome parameter of calculations:

$$C_V = C_{s,c} \cdot SSA \cdot \rho, \tag{29}$$

where $\rho$ is the calculated density of the material.

$$\rho = \frac{m}{V_t} = \frac{m}{V_p + V_c} = \frac{m}{V_p + \dfrac{m}{\rho_c}}. \tag{30}$$

Here $m$ is the mass of the material, $V_t$ is the total volume of the material, $V_p$ the total volume of the pores in the material, $V_c$ is the volume of the compact part of the material, $\rho_c$ is the compact density of the material (e. g. the density of the non-porous material; in calculations $\rho_c = 2$ g/cm$^3$, which is a typical value for the compact graphite materials). Parameters $m$ and $\rho_c$ are fixed model parameters (see Table), while $V_p$ is calculated similarly to $A_p$ (13):

$$V_p = \pi \cdot N_1(d_1^2 l_1 + \beta_{12} d_2^2 l_2 + \beta_{12}\beta_{23} d_3^2 l_3). \tag{31}$$

The impedance $\mathbf{Z}_p$ is calculated for the wide range of frequencies $f$: from 0.1 mHz to 100 kHz. The most relevant range of $f$ for the operation of supercapacitors is from ca. 0.1 Hz to ca. 100 Hz (or the range of $\log_{10} f$ is from $-1$ to 2).

Below the influence of various structural parameters of a porous system on its electrochemical properties, in particular, $C_V$, is analyzed. In order to decrease the number of varied parameters, the diameters of different generations of the pores $d_1$, $d_2$, $d_3$ and the length of the 1$^{\text{st}}$ generation of pores $l_1$ are fixed. Thus, the computations are focused on the influence of $l_2$ and $l_3$, as well as the total pore length and the branching factors $\beta_{12}$, $\beta_{23}$.

### 3.1. Simple model systems: effects of pore diameter, geometry, and branching

At first, the generalized staircase model was applied to the simple configurations of pores depicted in Fig. 7.

The results of the calculations for the model systems A, B, and C, containing 1 type of pores ($\beta_{12} = \beta_{23} = 0$), are shown in Fig. 8. The pore length was $l = 3.2$ $\mu$m. The results were presented as the Nyquist plots of impedance ($-\mathrm{Im}(\mathbf{Z})$ vs. $\mathrm{Re}(\mathbf{Z})$) and the Bode plots of $C_V$.

The Nyquist plots demonstrate the expected transition from $\phi = 45°$ at the frequencies higher than the threshold value $f_0$ to $\phi = 90°$ at the frequencies $f < f_0$. The threshold $f_0$ decreases with the pore diameter (11). In the Bode plots one observes the transition from the constant $C_V$ at $f < f_0$ to the varying $C_V$, which decreases with the frequency $f > f_0$. As expected, the narrower pores have higher values of $C_V$ due to the higher density of the material: $\rho = 1.513$ g/cm$^3$ for $d = 0.7$ nm, $\rho = 0.136$ g/cm$^3$ for $d = 30$ nm. The narrower

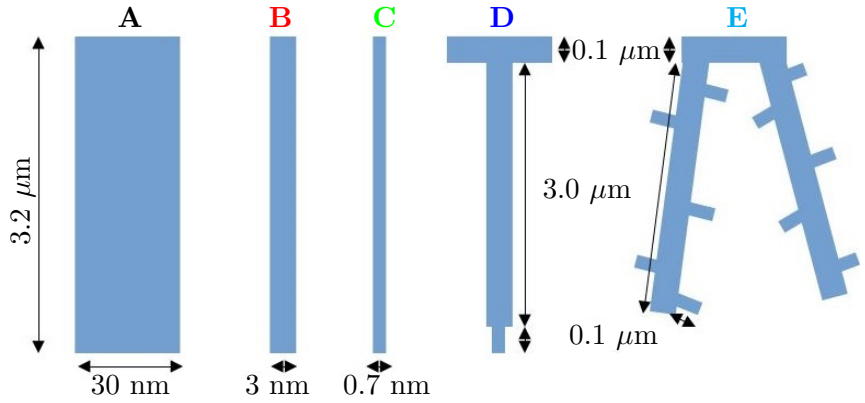


Fig. 7. The sketches of the simple pore model systems

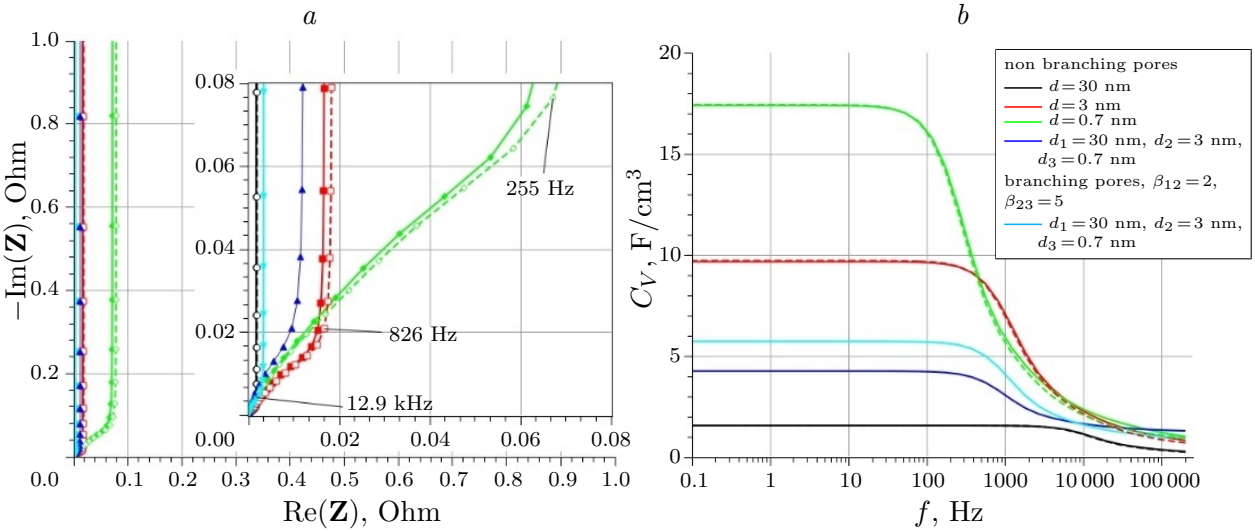


Fig. 8. The Nyquist plots ($a$) and the Bode plots ($b$) of the model systems. Dashed lines: the model systems with 1 generation of pores ($\beta_{12} = \beta_{23} = 0$) and various pore diameter $d$. Solid lines (except blue and cyan): the model systems with 3 generations of non-branching pores ($\beta_{12} = \beta_{23} = 1$) and the same pore diameter $d$. Blue lines: the model system with non-branching pores and decreasing pore diameters. Cyan line: the model system with branching factors $\beta_{12} = 2$, $\beta_{23} = 5$ and decreasing pore diameters

pores also have a lower threshold frequency $f_0$ and a stronger loss of $C_V$ with increase of $f$. Thus, at certain $f > f_0$, for the pores with $d = 3$ nm, the values of $C_V$ are predicted to be higher than the values for the pores with $d = 30$ nm (Fig. 8, $b$).

In order to validate the model, these results are compared with calculations for the model system with 3 generations of non-branching ("consecutive") pores ($\beta_{12} = \beta_{23} = 1$) with the same diameter $d_1 = d_2 = d_3$ (Fig. 8). For the data in Fig. 8, the lengths of the pores of the 1$^{st}$, 2$^{nd}$, and 3$^{rd}$ generations are $l_1 = 0.1$ $\mu$m, $l_2 = 3$ $\mu$m, $l_3 = 0.1$ $\mu$m. The total length of a single pore for the given model system is $l_p = l_1 + l_2 + l_3 = 3.2$ $\mu$m, which is the same as in the model system with 1 generation of pores.

As expected, the results of the calculations for these two model systems coincide well except for a slight negligible deviation observed in the Nyquist plots for low frequencies. This slight deviation characterizes a small and acceptable inaccuracy of the new model with 3 generations related to the uniform spreading of the impedance of branch pores over the length of a parent pore.

It was also verified that if all 3 generations of non-branching pores have the same diameter, then the results were the same for all models with the same total pore length, independently of the relative lengths of pores of each generations. Indeed, the results of calculations for the model system with $l_1 = 3$ $\mu$m, $l_2 = l_3 = 0.1$ $\mu$m coincide with the results for the model systems with $l_1 = l_3 = 0.1$ $\mu$m, $l_2 = 3$ $\mu$m, and $l_1 = l_2 = 0.1$ $\mu$m, $l_3 = 3$ $\mu$m.

The results for the model system D with non-branching pores, with different diameters $d_1 = 30$ nm, $d_2 = 3$ nm, $d_3 = 0.7$ nm and the lengths $l_1 = l_3 = 0.1$ $\mu$m, $l_2 = 3$ $\mu$m are shown in Fig. 8 as blue lines. The Nyquist plots for this model system show a more complex behavior, indicating the influence of all 3 generations of the pores. The phase shift angle $\phi$ is larger than 45° even at relatively high frequencies, while the transition to the behavior with $\phi = 90°$ is less sharp comparing to the system with $d = 3$ nm (red lines). Such behavior of the Nyquist plots is similar to the one predicted for the conical pores with decreasing diameter [8].

In comparison to the system B with straight pores, the system D with wide pore openings has a significantly lower density (0.841 and 0.372 g/cm$^3$ correspondingly). Thus, if the frequencies $f$ are not too high, then the system D shows the lower values of $C_V$. The threshold frequency $f_0$ for this system is close to the model system B with $d = 3$ nm (red line), despite of the narrower apex of the pores of the system D ($d_3 = 0.7$ nm). A narrower apex is expected to result in a lower $f_0$, however, this effect is weak and undetectable. On the other hand, due to a wider mouth of the pore $d_1 = 30$ nm, the decrease of $C_V$ in high frequency range is significantly lower in comparison to the system B ($d = 3$ nm). Above a certain frequency, the values of $C_V$ of the system D with wide pore openings are bigger than those of the system B with straight pores.

Finally, the results for the model system E with the same dimensions of 3 generations of pores as in the system D, but with the branching factors $\beta_{12} = 2$ and $\beta_{23} = 5$, are shown in Fig. 8 (cyan lines). As a branching pore has a higher surface area than a non-branching pore, the number of pores in the system E is lower than in the system D. This results in a higher density (0.498 and 0.372 g/cm$^3$ correspondingly), and, thus, higher values of $C_V$. Also, the value of the threshold frequency $f_0$ of the system E falls in the interval between the values for the systems with 1 generation of pores and the diameters $d = 3$ and $d = 30$ nm.

This proves that the modelled branching porous structure is more favorable for efficient surface utilization than a non-branching structure at least in the considered frequency range. The increased efficiency can be qualitatively explained by the fact that for the same frequency $f$, and thus, the same penetration depth $\lambda$, the system with $\beta_{12} = 2$ has ca. 2 times higher surface area than a system with non-branching pores. However, for high frequencies, the efficiency of non-branching pores becomes comparable with branching pores. This can be explained by a stronger contribution of the wider mouths of pores to the total pore surface area in the non-branched pores.

Summing up, the following conclusions are made from the comparison of the models A–E.

- Straight and narrow (micro-)pores provide the highest interfacial capacitance at least at moderate potential modulation rates. For the applications requiring high power output (fast discharging rates), narrow mesopores might be more efficient than micropores.
- The presence of wide opening of the pores ("hierarchical" pores: wider pores transforming to the narrower ones) results in the smaller losses of capacitance with the potential modulation rate increase. However, the material density and the related val-

ues of $C_V$ decrease. Thus, the wide opening of the pores might be not favorable for the applications requiring a high energy density.

- Comparing to a system with non-branching pores, the system with branching pores and same pores dimensions has a similar dependence of capacitance on the modulation rate. However, pores branching results in a higher material density (lower porosity) for the same SSA and higher values of $C_V$. Therefore, the branching of pores appears to be favorable for better material performance as supercapacitor electrodes.

In the next Subsection the influence of the structure of porous systems, namely, the pores diameter, length, and branching factors on the material performance is analyzed in details.

## 3.2. Evaluation of influence of structural porosity parameter on material efficiency

### 3.2.1. Effect of pore "mouth"

First, the systems with the same total length of the non-branching pores $l_p = l_1 + l_2 + l_3 = 1.2$ $\mu$m were modelled (see Fig. 9). The system F1 with the straight micropores with the diameter $d = 0.7$ nm was compared to the systems F2–F4 with wide pore openings, modelled as short (0.1 $\mu$m) segments with various diameters at the mouths of pores. The comparison of the results for the systems F1–F4 is given in Fig. 10.

The Nyquist plots of the system with straight pores with $d = 0.7$ nm (black lines in Fig. 10) show the typical behavior described in the Subsection 3.1: a transition from $\phi = 45°$ at $f > f_0$ to $\phi = 90°$ at $f < f_0$. For the same threshold $f_0$, the Bode plots show the transition in the behavior of $C_V$: from the independence of $f$ for $f < f_0$ to the decrease with increase of $f$ for $f > f_0$.

Adding the short wide opening segments to the mouths of the pores shifts $f_0$ to slightly higher frequencies and decreases the loss of $C_V$ at higher $f$. These effects are stronger for wider openings. On the other hand, the presence of a wide opening increases the material porosity and decreases the material density: $\rho = 1.51$, 1.23 and 0.175 g/cm$^3$ for the systems F1 (no wider opening), F2 (opening segment with $d = 3$ nm) and F3 (opening segment with $d = 30$ nm) correspondingly. The lower density results in the lower values of $C_V$ at low and moderate frequencies. Thus, under low and moderate potential modulation rates the pores without wide openings are more favorable for supercapacitors.

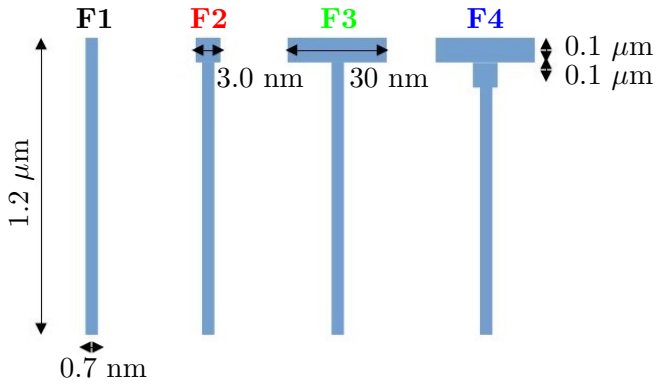


Fig. 9. The sketches of the pore model systems F1–F4

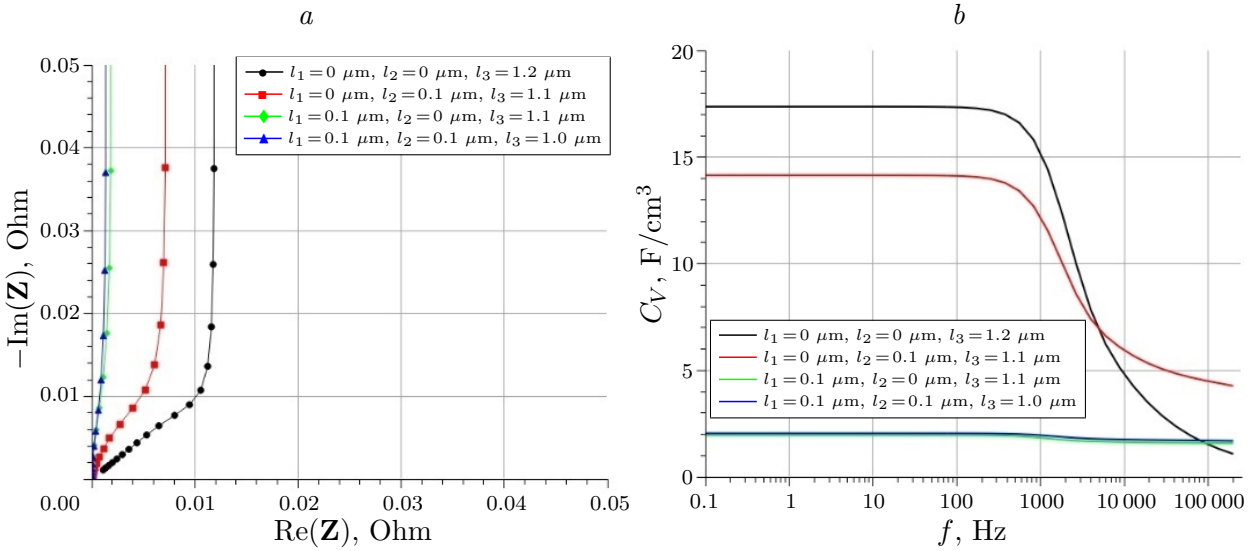


Fig. 10. The Nyquist plots ($a$) and the Bode plots ($b$) of the model systems with 3 generations of non-branching pores with the diameters $d_1 = 30$ nm, $d_2 = 3$ nm, $d_3 = 0.7$ nm. The relative lengths of the segments were varied, while the total pore length was kept constant $l_p = l_1 + l_2 + l_3 = 1.2$ μm

### 3.2.2. Influence of pores branching

In order to evaluate the effect of pores branching on the capacitance of porous materials, the sets of systems with pores of the same dimensions ($l_1 = 0.1$ μm, $d_1 = 30$ nm, $l_2 = 3.0$ μm, $d_2 = 3$ nm, $l_3 = 0.1$ μm, $d_3 = 0.7$ nm) and varied branching factors are modelled. The first set (G) has the fixed $\beta_{23} = 5$ and varied $\beta_{12}$ from 1 to 100, and the second set (H) has the fixed $\beta_{12} = 5$ and varied $\beta_{23}$ from 1 to 100 (Fig. 11). The Bode plots are shown in Fig. 12.

For all model systems, very close values of $f_0$ are obtained, close to one of the system B (pores with $l = 3.2$ μm, $d = 3$ nm, red lines in Fig. 8). The increase of branching factors increases the loss of $C_V$ at high potential modulation rates. However, it also increases the density of the material. For example, for $\beta_{23} = 5$ the increase of $\beta_{12}$ from 1 to 10 and further up to 100 results in the increase of the material density from 0.375 to 0.734 and further up to 0.840 g/cm$^3$.

It may seem to be counter-intuitive that a system with stronger pore branching has a higher density. However, it can be rationalized as follows. Pore branching results in higher surface area of each individual pore, and thus, for the same SSA, a smaller amount of pores is required. This means the lower porosity and the higher density of the material. The

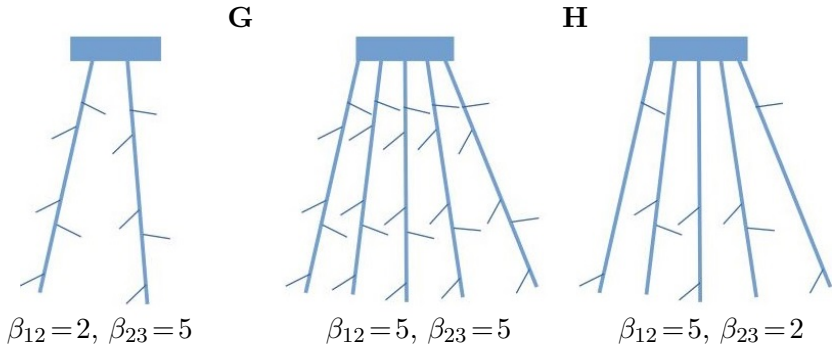


Fig. 11. The sketches of the model system sets G and H

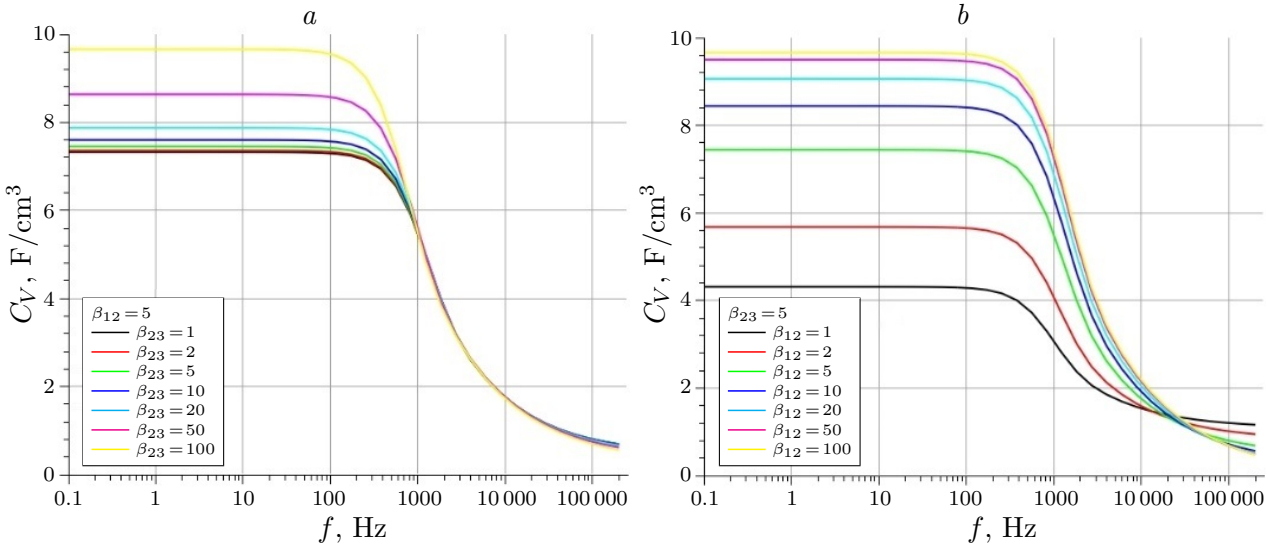


Fig. 12. The Bode plots for the systems G with varied $\beta_{12}$ ($a$) and the systems H with varied $\beta_{23}$ ($b$). The lengths of the pores are: $l_1 = 0.1$ $\mu$m, $l_2 = 3.0$ $\mu$m, $l_3 = 0.1$ $\mu$m

effect of the increased material density is predominant in the wide range of $f$. Only at very high $f$ (above 10 kHz) the materials with a lower $\beta_{12}$ demonstrate a higher $C_V$. For the increase of $\beta_{23}$, the effect of stronger loss of $C_V$ at higher frequencies is even less pronounced. This is explained by the fact that the contribution of terminal pores is smaller at the higher frequencies due to the short modulation penetration depth.

Thus, it is concluded that in general pore branching is a favorable strategy to increase the capacitance of porous materials for supercapacitors with non-faradaic impedance, for example for the EDLC.

Below the model predictions for the systems with faradaic impedance are evaluated. These systems are relevant for the electrode materials for pseudocapacitors.

### 3.3. Influence of faradaic impedance

The generalized staircase model was applied to calculate the impedance of porous electrodes with faradaic impedance involved in energy storage. The interfacial impedance in this case was modelled as the impedance of a parallel connection of the capacitive impedance $\mathbf{Z}_{dl} = \mathbf{Z}_{C=C_{dl}}$ and the faradaic impedance $\mathbf{Z}_f = R_{ct} + \mathbf{Z}_{C=C_{ps}}$ (Fig. 13).

The Nyquist plots clearly shows the influence of the faradaic impedance, especially at low frequencies, even for the relatively low values of $i_0$ (the exchange rate of electrochemical reaction), i. e. for the relatively high $R_{ct}$ (5). As the rate $i_0$ increases, the predominance of $\mathbf{Z}_f$ over $\mathbf{Z}_{dl}$ becomes pronounced also at higher frequencies. However, the Bode plots show that the contribution of $C_{ps}$ becomes significant only for high $i_0$ and for low or moderate frequencies. For example, for the system with a very fast charge transfer rate ($i_0 = 50$ mA/cm$^2$) and high $C_{ps} = 300$ $\mu$F/cm$^2$, the contribution of $C_{ps}$ becomes noticeable only at $f < 100$ Hz, even though the $|\mathbf{Z}_{dl}| > |\mathbf{Z}_f|$ already at $f < 1000$ Hz.

Fig. 14 compares the Nyquist and the Bode plots for the porous systems with varied branching factor $\beta_{23}$, while $\beta_{12} = 2$ was fixed. The Nyquist plots are practically identical, except slight deviations observable in the high frequency range (see inset of Fig. 14, $a$). It has to be reminded that data in the Nyquist plots, namely, $-\mathrm{Im}(\mathbf{Z_p})$ vs $\mathrm{Re}(\mathbf{Z_p})$, do not

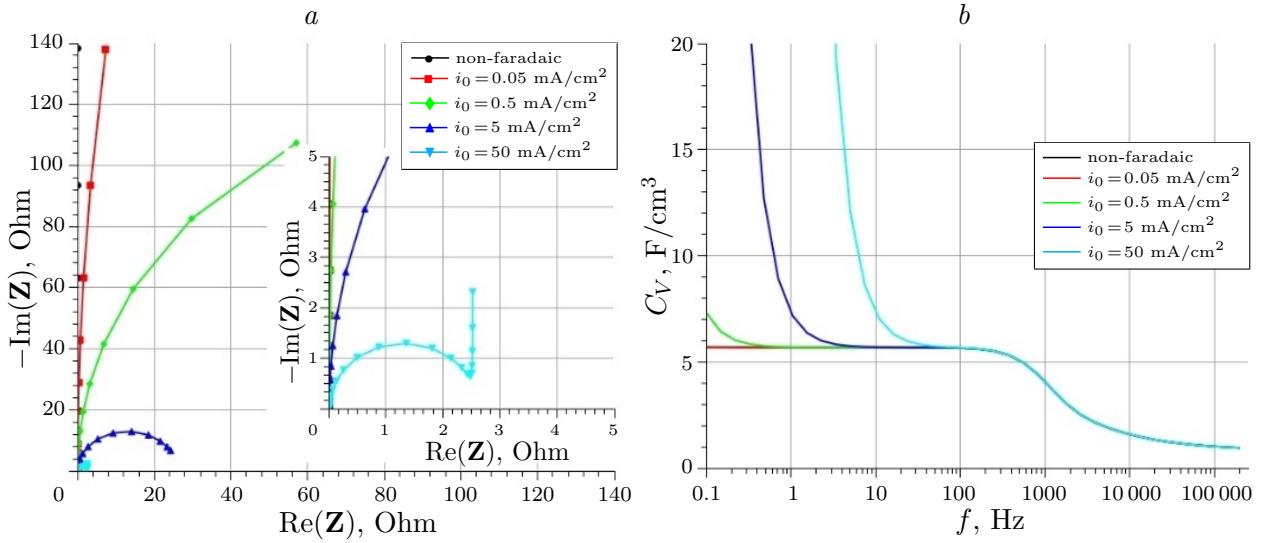


Fig. 13. The Nyquist plots ($a$) and the Bode plots ($b$) for the model system with typical structural parameters: $d_1 = 30$ nm, $l_1 = 0.1$ $\mu$m, $d_2 = 3$ nm, $l_2 = 3$ $\mu$m, $d_3 = 0.7$ nm, $l_3 = 0.1$ $\mu$m, $\beta_{12} = 2$, $\beta_{23} = 5$, in the presence of the faradaic impedance

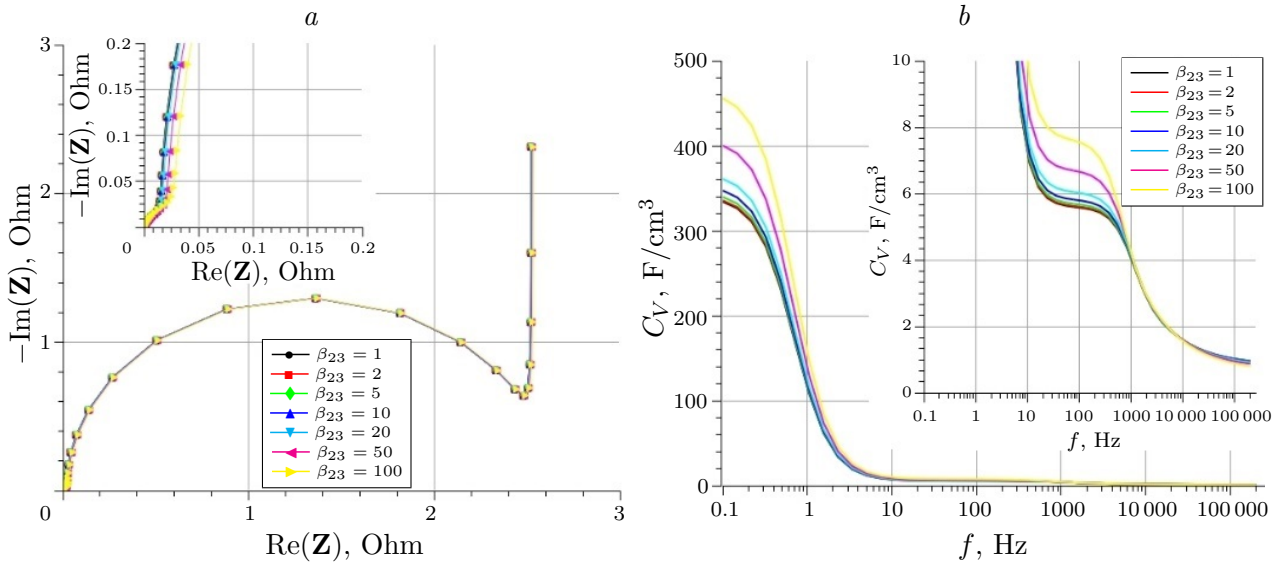


Fig. 14. The Nyquist plots ($a$) and the Bode plots ($b$) for the model system with faradaic impedance ($C_{ps} = 300$ $\mu$F/cm$^2$, $i_0 = 50$ mA/cm$^2$) for the varied branching factor $\beta_{23}$ ($\beta_{12} = 2$ was fixed)

reflect the changes in material porosity. This shows that the influence of branching factor on the total impedance in the presence of the faradaic impedance is negligible. It can be explained by the fact that faradaic impedance becomes predominant in the low frequency range, where the penetration depth $\lambda$ is close or larger than the pore length $l_p$ and the effects of pore geometry are weak. In this case, one can expect that the main effect of branching factor increase on the capacitance of the materials with faradaic impedance is related to the changes in the material porosity and density. Indeed, the Bode plots in Fig. 14 demonstrate a significant increase of the values of $C_V$ related to the increase of the material density from $\rho = 0.486$ g/cm$^3$ for $\beta_{23} = 1$ to $\rho = 0.663$ g/cm$^3$ for $\beta_{23} = 100$.

## 4. Conclusions

It was demonstrated that the new generalized staircase model allows to describe the impedance of the porous materials with complex pore geometry. The pore geometry can include a system of hierarchical pores, e. g. wide pores transforming into single narrower pores or branching into multiple narrower pores evenly distributed over a parent pore. Modelling of the interfacial impedance of an individual pore can be done by splitting a pore into a number of segments and using the recursive equations to calculate the impedance of a part of a pore by sequentially including all segments. The generalized staircase model allows to calculate the impedance of a single pore and the total impedance of all pores for the material with both non-faradaic and faradaic processes.

The generalized staircase model allows to evaluate the influence of structural parameters of the porous electrode materials on their electrochemical performance in supercapacitors. It was demonstrated that the volume specific capacitance $C_V$ serves as an informative parameter of the electrochemical performance.

The variation of the structural parameters of the model porous systems causes two groups of effects on the capacitance of materials.

The first group of effects is related to the limited depth of the penetration of potential modulation. These effects are manifested as a decrease of capacitance at modulation frequencies above the threshold value $f_0$. Both the magnitude of this decrease and the value of $f_0$ depend on the structure of a porous system. In particular, a decrease of the pore diameter and an increase of the pore length result in the stronger loss of $C_V$ and an increase of the value of $f_0$. Thus, the electrochemical performance of the material decreases. On the other hand, a wider opening of pores (e. g. hierarchical pores) decreases the loss of $C_V$ at high frequencies.

The second group of effects is related to the change in material density caused by the changes in the parameters of a porous system. A higher porosity results in a lower density of the material, a lower volume specific capacitance $C_V$ and a lower energy density. These effects are often counter-acting the effects of the first group.

The new generalized staircase model allows to evaluate the influence of these two groups of effects and detect the predominant effect for a chosen set of the structural parameters. It was observed that excessively wide opening of the pores results in a strong density decrease and lower values of $C_V$. On the other hand, an increase of pore branching results in the predominant effect of an increase of material density and, thus, in higher values of $C_V$. The latter effect is the most important effect for the capacitor electrode materials with faradaic interfacial reactions, i. e. pseudocapacitors. The faradaic impedance is predominant at lower rates of potential modulation (low $f$), where the effects of the first group are weak.

The results of the modelling provide the guidelines for the focused design of electrode materials with high performance in electrochemical double layer supercapacitors and pseudocapacitors.

**Acknowledgements.** The work is supported by CNRS (grant No. MMO-GRACE-2019) and Mica-Carnot (grant No. COM-Gra-2020).

## References

[1] **Diesendorf M., Elliston B.** The feasibility of 100 % renewable electricity systems: A response to critics. Renewable and Sustainable Energy Reviews. 2018; (93):318–330. DOI:10.1016/j.rser.2018.05.042.

[2] **Simon P., Gogotsi Yu., Dunn B.** Where do batteries end and supercapacitors begin? Science. 2014; 343(6176):1210–1211. DOI:10.1126/science.1249625.

[3] **Gogotsi Yu., Simon P.** True performance metrics in electrochemical energy storage. Science. 2011; 334(6058):917–918. DOI:10.1126/science.1213003.

[4] **MacDonald D.D.** Reflections on the history of electrochemical impedance spectroscopy. Electrochimica Acta. 2006; 51(8–9):1376–1388. DOI:10.1016/j.electacta.2005.02.107.

[5] **Damaskin B.B., Petrii O.A., Tsirlina G.A.** Development of models of electrical double layer. Electrochemistry. Moscow: Chemistry; 2001: 350–353. (In Russ.)

[6] **Prieto F., Alvarez-Malmagro J., Rueda M.** Electrochemical impedance spectroscopystudy of the adsorption of adenine on Au(111) electrodes as a function of the pH. Journal of Biomechanics. 2017; 793(111):209–217. DOI:10.1016/j.jelechem.2017.03.021.

[7] **De Levie R.** On the impedance of electrodes with rough interfaces. Journal of Electroanalytical Chemistry. 1989; 261(1):1–9. DOI:10.1016/0022-0728(89)87121-9.

[8] **Keiser H., Beccu K.D., Gutjahr M.A.** Abschätzung der porenstruktur poröser elektroden aus impedanzmessungen. Electrochimica Acta. 1976; 21(8):539–543. DOI:10.1016/0013-4686(76)85147-X. (In Germ.)

[9] **Candy J.-P., Fouilloux P., Keddam M., Takenouti H.** The characterization of porous electrodes by impedance measurements. Electrochimica Acta. 1981; 26(8):1029–1034. DOI:10.1016/0013-4686(81)85072-4.

[10] **Eikerling M., Kornyshev A.A., Lust E.** Optimized structure of nanoporous carbon-based double-layer capacitors. Journal of the Electrochemical Society. 2005; 152(1):E24–E33. DOI:10.1149/1.1825379.

[11] **Soboleva T., Zhao X., Malek K., Xie Zh., Navessin T., Holdcroft S.** On the micro-, meso-, and macroporous structures of polymer electrolyte membrane fuel cell catalyst layers. ACS Applied Materials and Interfaces. 2010; 2(2):375–384. DOI:10.1021/am900600y.

[12] **Chmiola J., Yushin G., Gogotsi Y., Portet C., Simon P., Taberna P.L.** Anomalous increase in carbon capacitance at pore sizes less than 1 nanometer. Science. 2006; 313(5794):1760–1763. DOI:10.1126/science.1132195.

[13] **Lopez L., Kim Y., Jierry L., Hemmerle J., Boulmedais F., Schaaf P., Pronkin S., Kotov N.A.** Electrochemistry on stretchable nanocomposite electrodes: Dependence onstrain. ACS Nano. 2018; 12(9):9223–9232. DOI:10.1021/acsnano.8b03962.

[14] **Eikerling M.** Water management in cathode catalyst layers of PEM fuel cells. Journal of the Electrochemical Society. 2006; 153(3):E58–E63. DOI:10.1149/1.2160435.

[15] **Housseinou B., Wang W., Pronkin S., Romero T., Baaziz W., Nguyen-Dinh L., Chu W., Ersen O., Pham-Huu C.** Biosourced foam-like activated carbon materialsas high-performance supercapacitors. Advanced Sustainable Systems. 2018; (1700123):1–12. DOI:10.1002/adsu.201700123.

Вычислительные технологии, 2020, том 25, № 6, с. 30–51. © ФИЦ ИВТ, 2020 ISSN 1560-7534
Computational Technologies, 2020, vol. 25, no. 6, pp. 30–51. © FRC ICT, 2020 eISSN 2313-691X

МАТЕМАТИЧЕСКОЕ МОДЕЛИРОВАНИЕ

DOI:10.25743/ICT.2021.26.5.004

# Обобщенная лестничная модель электрохимического импеданса пор в электродах суперконденсаторов

С. Н. Пронькин[1,*], Н. Ю. Шокина[2]

[1] Институт химии и процессов энергии, окружающей среды и здоровья, 67087, Страсбург, Франция

[2] Медицинский центр — Фрайбургский университет, 79106, Фрайбург, Германия

[*] Контактный автор: Пронькин Сергей Николаевич, e-mail: sergey.pronkin@unistra.fr

*Поступила 13 сентября 2021 г., принята в печать 21 сентября 2021 г.*

## Аннотация

Представлена новая обобщенная лестничная модель электрохимического импеданса для пористых материалов электродов в устройствах хранения энергии. Дано краткое описание существующих моделей межфазного импеданса и их ограничений. Новая модель основана на общепринятой "лестничной" модели импеданса цилиндрических пор. Однако новая модель учитывает сложную пористую структуру электродных материалов. В частности, модель описывает импеданс электродов с иерархической пористой разветвленной структурой, в которой широкие поры разветвляются в более узкие. Новая модель позволяет вычислить импеданс межфазной границы электрод/электролит в присутствии как нефарадеевских, так и фарадеевских процессов. Модель успешно опробована для пор с простой геометрией, для которых существуют точные решения. Изучено влияние структурных параметров модельных пористых электродов на их характеристики работы в суперконденсаторах. Проанализировано влияние диаметра пор, величины расширения начал пор и разветвления пор. Сформулированы критерии направленного дизайна электродных материалов для суперконденсаторов.

*Ключевые слова*: лестничная модель, межфазный импеданс, рекурсивные уравнения, модельные системы.

*Цитирование*: Pronkin S.N., Shokina N.Yu. Generalized staircase model of electrochemical impedance of pores in supercapacitor electrodes. Computational Technologies. 2021; 26(5):30–51. DOI:10.25743/ICT.2021.26.5.004.

**Благодарности.** Исследование выполнено при поддержке Национального центра научных исследований (грант № MMO-GRACE-2019) и Mica-Carnot (грант № COM-Gra-2020).